LUBRICATION SCIENCE Tribotest
Lubrication Science 2010; **22**:195–205
Published online 28 May 2010 in Wiley InterScience (www.interscience.wiley.com). DOI: 10.1002/ls.125

The critical condition for intrusion of a steel ball into sliding contact space

Fuxun Li, Dongfeng Diao*,† and Xue Fan

Key Laboratory of Education Ministry for Modern Design and Rotor-Bearing System, School of Mechanical Engineering, Xi'an Jiaotong University, Xi'an 710049, China

ABSTRACT

The intrusion tests of a ball into sliding contact space were carried out. A stainless steel ball with 3.175 mm radius was used as a sphere particle to study the critical intrusion condition of the ball into the contact space between the organic glass and the polyurethane rubber. The effect of intrusion angle of the contact space and the friction coefficients among the ball, the organic glass and the polyurethane rubber on the critical condition were studied experimentally. Then, the intrusion conditions for the ball into the contact space were analysed theoretically. The results showed that the calculated critical intrusion angles agreed well with the experimental ones. Finally, the intrusion diagram as a function of critical intrusion angle, friction coefficient μ_1 and μ_2 (here, μ_1 is the friction coefficient between the ball and the polyurethane rubber, μ_2 is the friction coefficient between the ball and the organic glass) was introduced to evaluate the intrusion performance of a ball into the sliding contact space. Copyright © 2010 John Wiley & Sons, Ltd.

Received 27 September 2008; Revised 23 March 2010; Accepted 12 April 2010

KEY WORDS: sliding contact space; ball; intrusion; critical intrusion angle; critical normal load

INTRODUCTION

Organic photoconductor (OPC)-blade tribosystem is a very important system as a typical sliding contact interface in printer. When the printer finishes a round of printing, there are a number of leftover toner particles attached to the surface of OPC. These leftover particles are harmful to the next round of printing. On the other hand, there are many atomy particles in the working environment that also affect the printing quality through the abrasive to the OPC-Blade tribosystem.[1,2] Although some scientists studied the performance of particles at spaces about abrasive flow machining,[3–7] the research on particles intruding into contact space is very few.

The intrusion of particles into a contact space was dependent on the sizes of the particles, the normal load, the friction coefficient and the intrusion angle.[8,9] Fang *et al*. studied the movement pattern of

*Correspondence to: Dongfeng Diao, Key Laboratory of Education Ministry for Modern Design and Rotor-Bearing System, School of Mechanical Engineering, Xi'an Jiaotong University, Xi'an 710049, China.
†E-mail: dfdiao@mail.xjtu.edu.cn

the particle during intrusion process and the results showed that the movement pattern is dependent on the particle size and normal force. The movement pattern of particles has great influence on the abrasion pattern.[8] The effects of surface texture and particle size on the possibility of particle intrusion into a contact space were given using a designed head/Disk tribometer.[9] Hokkirigawa and Kato carried out experimental and theoretical investigation of ploughing, cutting and wedging formation and introduced the degree of penetration as an index to describe the wear mode diagram that showed the possible region of abrasive intrusion during a hard indenter sliding against the soft materials.[10] Briscoe pointed out that scratching in brittle friction interface may scratch chips off from the interface, and the chips were considered as particles.[11] Challen and Oxley built a cutting model with chips (wear particles) for rougher surfaces.[12] The performance of nanoparticles intruding into OPC-Blade tribosystem has been investigated in some experiments using an OPC-Blade tribosystem in printer.[13] However, there is no reported experimental method to study the performance of single particle intruding into sliding contact space. The intrusion condition of a particle into the contact space and the relationships between intrusion angle and friction coefficients of particle against two contact surfaces are not clear yet.

We have studied the intrusion pattern of single particle into Roller-Scraper tribosystem by using static non-adhesion contact model.[14] The results showed that the dominant movement patterns of the particles with different sizes were sliding and rolling. The results also indicated that the friction and wear performance of the roller was mostly dependent on the intrusion pattern of particles. Therefore, the purpose of present study is to elucidate the intrusion condition and introduce the intrusion diagrams of particle as a function of friction coefficients and critical intrusion angles using a designed tribotester.

EXPERIMENT AND THEORETICALLY ANALYSIS

Experimental apparatus

Figure 1 shows the sketch of the designed tribotester. The tribotester contains four main parts: the static plate (polyurethane rubber) and its holder; the ball (stainless steel) and its loading control; the rotary disk (organic glass) and its driving system; and the signal collecting system. The underside surface of the static plate is defined as surface 1, which is inclined, and the upside surface of the rotary disk is defined as surface 2, which is placed horizontally. Therefore, a wedge type space between the two surfaces is formed as shown in Figure 1b. The holder of the static plate is fixed on stage 1 with a bearing in it, and the included angle of the wedge type space can be adjusted by locking the holder at different positions in the arc guide groove with a screw bolt and nut.

The ball is in the wedge type space contacting with both surface 1 and surface 2. A leader is used to connect the ball by perforating one end of the leader across the centre of the ball. The other end of the leader is connected with the connecter by bearing 3 (Figure 1c), therefore the ball can roll with the leader. However, when the leader is locked by lock bolt 4, the leader and the ball will be fixed on the connecter without rolling. A beam is used to connect the connector to stage 2. One tip of the beam is connected with the connector by shaft 2 and bearings 2 (Figure 1c). When Shaft 2 is locked by lock bolt 3, the connecter is fixed on the tip of the beam. The other tip of the beam is connected with stage 2 by shaft 1 and bearings 1 (Figure 1d), so the beam can sway horizontally. But when shaft 1 is locked by lock bolt 2, the beam is fixed on stage 2. Both stage 1 and stage 2 can move along x,

DOI: 10.1002/ls

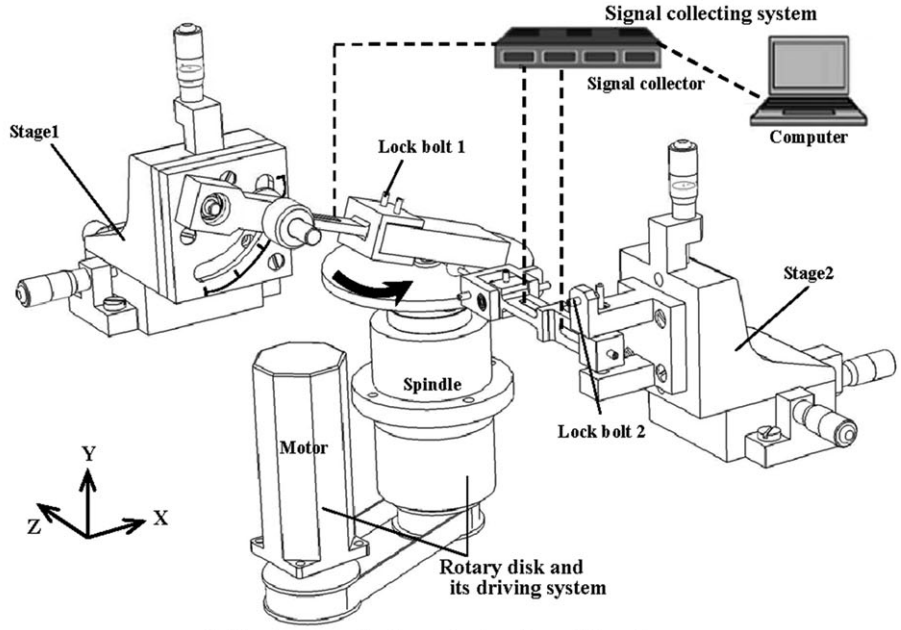

(a) The integrated schematic drawing of the tribotester

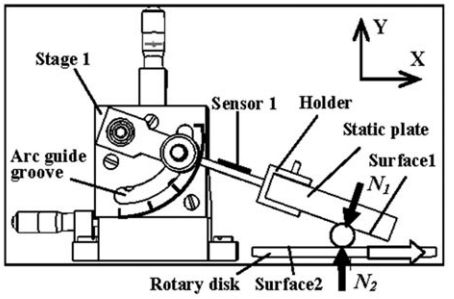

(b) Structure of the static plate and its holder

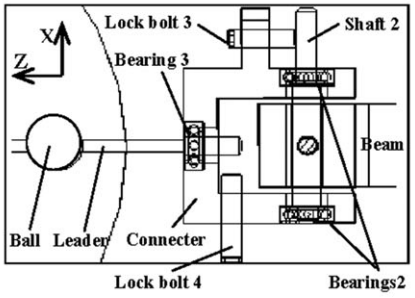

(c) Connect method of ball, connector and beam

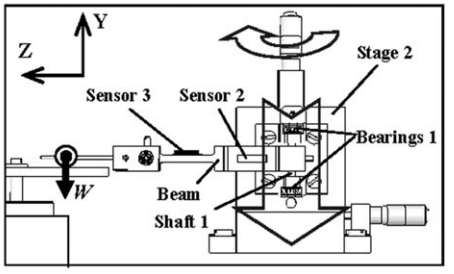

(d) The ball and its loading control

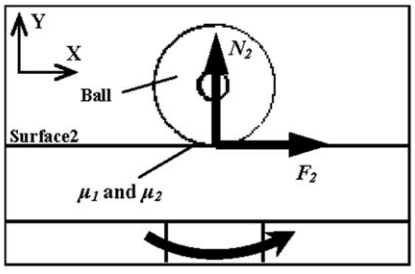

(e) Measurement of μ_1 and μ_2

Figure 1. The sketch of the tribotester of ball intrusion into sliding contact space 178 × 263 mm (300 × 300 dpi).

DOI: 10.1002/ls

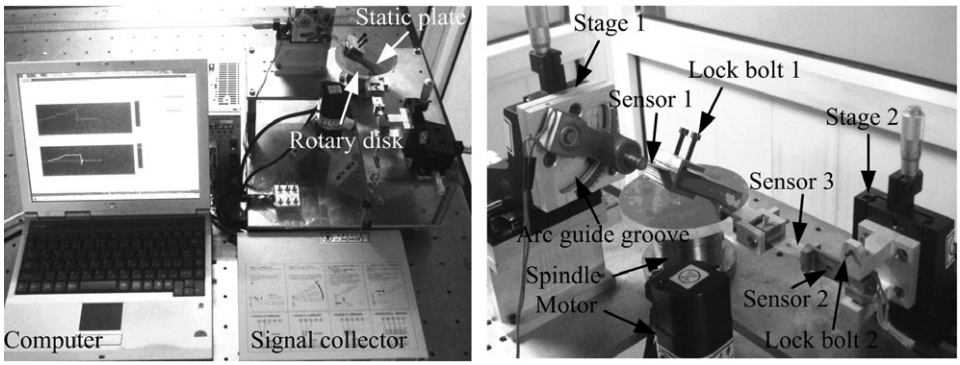

Figure 2. The tribotester of ball intrusion into sliding contact space 165 × 60 mm (300 × 300 dpi).

y and *z* directions. The rotary disk is fixed on the spindle of the driving system, which is driven by servo motor (Figure 1a). The signal collecting system contains the signal collector, the computer and sensors 1, 2 and 3 (Figure 1a). Sensor 1 is stuck on the holder of the static plate that can detect the normal force N_1 between the ball and surface 1. Sensor 2 and sensor 3 are on the beam. Sensor 2 is used to detect the friction force F_2 between the ball and surface 2, sensor 3 is used to detect the normal load W loaded in the centre of the ball. The normal load is loaded by adjusting stage 2 downwards along *y* direction (Figure 1d). Figure 2 shows the actual equipment used for the tests of a ball intrusion into sliding contact space.

Experimental procedure

The friction coefficient between the ball and surface 1 is μ_1 and that between the ball and surface 2 is μ_2. In the experiment of measuring the values of μ_2, adjust stage 1 and the angle holder to put surface 1 away from the ball (Figure 1e). Then adjust the connecter to let leader parallel to surface 2 and tighten lock bolt 3 to fix he connecter; tighten lock bolt 4 to fix the leader and adjust the beam to the place where the leader dead against the revolving centre of surface 2 and tighten lock bolt 2 to fix the beam. Under this situation, the ball can not roll and the beam can not sway. When surface 2 is revolved by the motor, adjust stage 2 downwards to let the ball touch surface 2. The friction force F_2 from surface 2 and the normal load W loading in the centre of the ball are detected by sensors 2 and 3 respectively, and recorded by the signal collector and computer. Because surface 1 is not contacted with the ball, the value of normal load W is equal to the normal force N_2 between surface 2 and the ball. The value of friction coefficient μ_2 can be calculated by N_2 and F_2 as follow:

$$\mu_2 = \frac{F_2}{N_2}$$

Changing the materials of the rotary disk with polyurethane rubber (the materials of the static plate) and using the same method mentioned earlier, the friction coefficient of surface 1 (μ_1) is obtained.

In the intrusion experiment of the ball into the sliding contact space, adjust the holder to a specified angle and lock it. Adjust stages 1 and 2, and put the ball, surfaces 1 and 2 at a suitable position where

DOI: 10.1002/ls

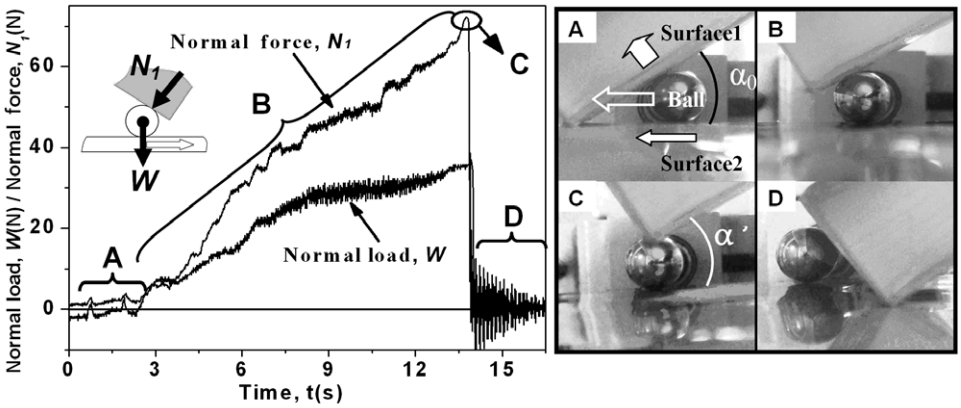

(a) The signals of W and N_1 (b) The entry process of the ball

Figure 3. Normal load putting on the centre of the ball and normal force between the ball and surface 2, 164 × 75 mm (300 × 300 dpi).

Table I. Experimental parameters.

Rotary disk material	Organic glass
Static plate material	Polyurethane rubber
Ball material	Stainless steel
Rotary disk rotate speed	50 rpm/min
Ball radius (r)	3.175 mm
Intrusion angle (α')	15°–35°
Normal load (W)	0–0.8 N
Friction coefficient between ball and surface 1 (μ_1)	0.08–0.38
Friction coefficient between ball and surface 2 (μ_2)	0.13–0.28

they just contact to each other but there are no normal forces acted among them (Figure 3a). Loosen lock bolts 2 and 4, the ball is free to roll and the beam is free to sway horizontally. Start the motor and adjust stage 2 downwards very slowly to put normal load W in the centre of the ball. Then, surface 2 will drive the ball move forward into the wedge type space between surfaces 1 and 2 (Figure 3b) with the augment of normal load W. The normal load W loaded in the centre of the ball and the normal force between the ball and surface 1 are detected by sensors 3 and 1, respectively (Figure 3). The augment of the normal load W continues until the ball getting across the wedge type space. The included angle between surfaces 1 and 2 is called entry angle α. During the movement of the ball, surface 1 is lifted up by the ball, and the entry angle α become smaller and smaller. The entry angle at the very beginning is defined as initial entry angle α_0 (Figure 3a). When the ball is on the point of getting across the space between surfaces 1 and 2, the entry angle reaches its minimum value. The smallest entry angle is named as the intrusion angle α' (Figure 3c), the normal load at this moment is called the intrusion normal load W'. The experimental parameters are listed in Table I.

DOI: 10.1002/ls

Theoretical analysis method

Figure 4 shows the theoretical analysis model for the intrusion of a ball into sliding contact space. Processes A, B, C and D in Figure 4 are corresponding to the processes in Figure 3b, 3a is the initial process of the ball's entry, B is halfway process, C is the critical process and D is the getting across process (intrusion). The rotary disk drives the ball entry into the wedge type space between surfaces 1 and 2. The angle between surface 1 and surface 2 is called entry angle α and the initial entry angle is defined as α_0. During the process, the entry angle gets smaller. At the moment of the ball getting across the space, the entry angle is defined as intrusion angle α'. The friction coefficient between the ball and surface 1 is μ_1 and between the ball and surface 2 is μ_2.

In order to analyse the intrusion performance of the ball into the sliding contact space, a force distribution of the ball for the case of Figure 4b is showed in Figure 5.

In x direction, the intrusion force F_X is as follows

$$x: \quad F_x = F_2 + F_1\cos\alpha - N_1\sin\alpha \tag{1}$$

In Y direction, the resultant force F_y acting on the ball is

$$y: \quad F_y = N_2 - F_1\sin\alpha - N_1\cos\alpha - W \tag{2}$$

The ball has no displacement in Y direction, $F_y = 0$. Therefore, according to $\mu = F/N$, from equations (1) and (2), we have the equation of the intrusion force F:

$$F = (\mu_2\cos\alpha + \mu_1\mu_2\sin\alpha - \sin\alpha + \mu_1\cos\alpha)N_1 + \mu_2 W \tag{3}$$

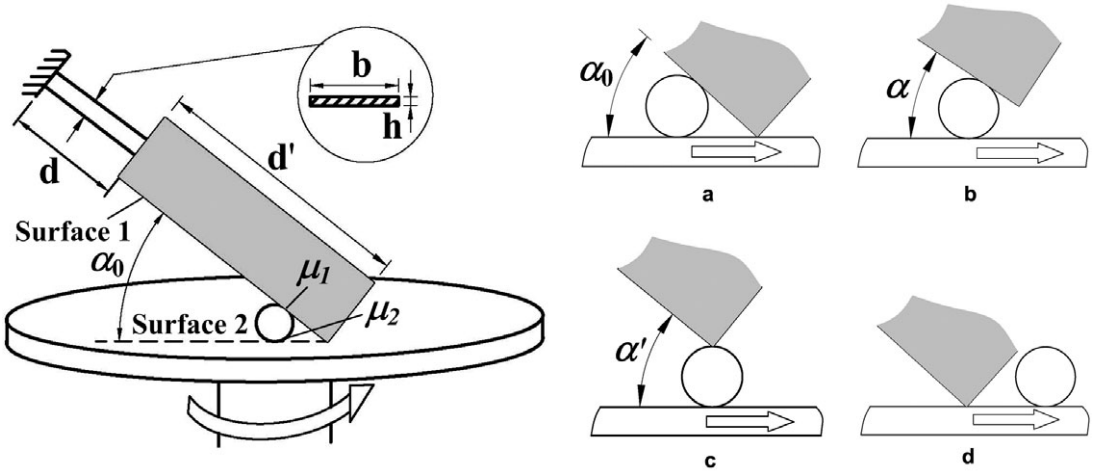

Figure 4. The sliding contact space model for simulating a ball intrusion into a space 161 × 71 mm (300 × 300 dpi).

DOI: 10.1002/ls

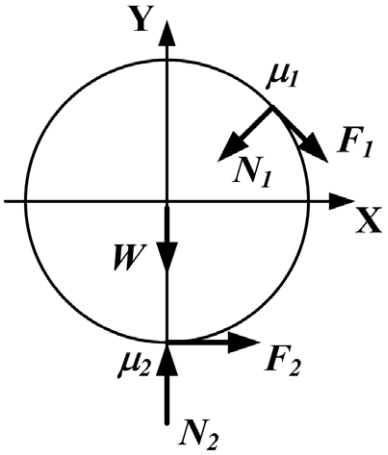

Figure 5. Force distribution at ball surface 56 × 69 mm (300 × 300 dpi).

where

$$N_1 = \left| \frac{EI(\alpha_0 - \alpha)}{dd'} \right|, \quad I = \frac{bh^3}{12} \tag{4}$$

Colligate equations (3) and (4), the intrusion force F of the ball on the point of getting across the wedge type space (when $\alpha = \alpha'$, $W = W'$) is

$$F = 5.76 \frac{\pi}{180} (\alpha_0 - \alpha')(\mu_2 \cos\alpha' + \mu_1\mu_2 \sin\alpha' - \sin\alpha' + \mu_1 \cos\alpha') + \mu_2 W' \tag{5}$$

When the intrusion force $F > 0$, the ball can intrude, and when $F < 0$ the ball can not intrude. Therefore, the condition of $F = 0$ is a key point of the intrusion. According to equation (5), when $F = 0$, the intrusion normal load W' acting on the ball is

$$W' = 5.76 \frac{\pi}{180} (\alpha_0 - \alpha')(\sin\alpha' - \mu_1\mu_2 \sin\alpha' - \mu_1 \cos\alpha' - \mu_2 \cos\alpha')/\mu_2 \tag{6}$$

When the value of intrusion normal load $W' = 0$ N, the intrusion angle α' is defined as the critical intrusion angle α_{cri}. According to equation (6), the relationship among critical intrusion angle α_{cri}, μ_1 and μ_2 is

$$\mu_1 = \frac{\tan\alpha_{cri} - \mu_2}{1 + \mu_2 \tan\alpha_{cri}} \tag{7}$$

DOI: 10.1002/ls

The critical intrusion angle α_{cri} is

$$\alpha_{cri} = \arctan \frac{\mu_1 + \mu_2}{1 - \mu_1 \mu_2} \tag{8}$$

RESULTS AND DISCUSSION

According to Figure 3, before the entry angle is reduced to the intrusion angle (process C in Figure 3), larger and larger normal load W is needed to keep the ball going forward. When the entry angle is equal to the intrusion angle, the normal load W and the normal force N_1 are both in maximum. Therefore, the moment when the ball is on the point of getting across the wedge type space as shown in Figure 4.C is greatly concerned in this study.

The data points in Figure 6 show the relationship between intrusion normal load W' and intrusion angle α'. According to Figure 6, if the values of μ_1 and μ_2 are both constants, the critical intrusion angle α_{cri} is existent. When the intrusion angle α' is less than the critical value α_{cri}, the effect of intrusion normal load W' on leading to the ball getting across is very small and unstable. When the intrusion angle α' is larger than the critical value, larger intrusion normal load W' is needed to cause the intrusion of the ball. The intrusion normal load W' increases as the intrusion angle increases. When the value of μ_1 is constant, the intrusion angle α' increases with the increasing of μ_2, this means that the intrusion of the ball becomes easier along with the increasing of μ_2.

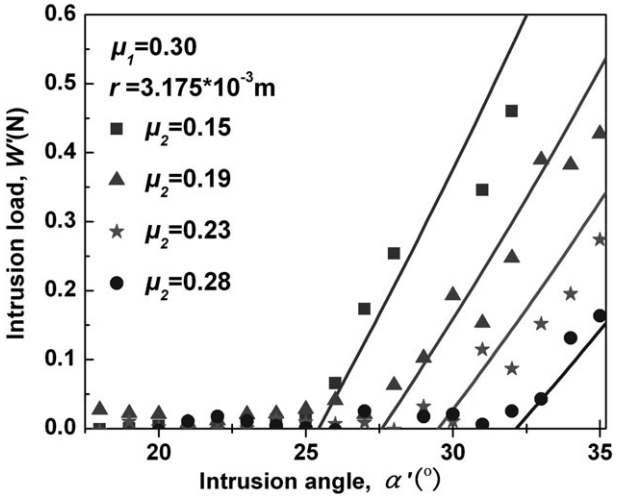

Figure 6. Experimental and calculating results of intrusin load and intrusion angle under different friction coefficients of μ_2, (μ_1 = 0.3) 150 × 118 mm (300 × 300 dpi).

DOI: 10.1002/ls

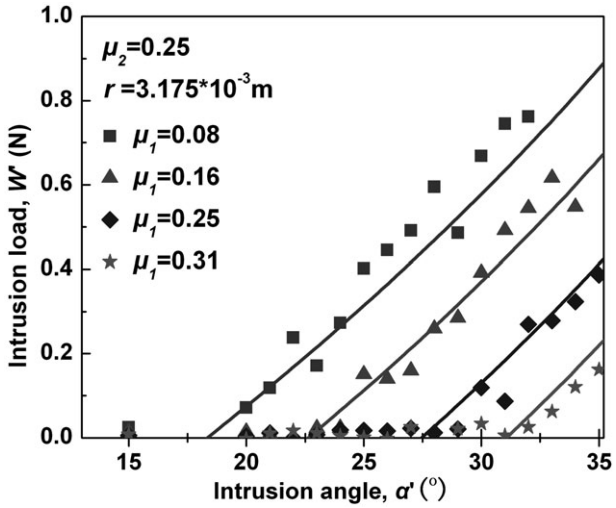

Figure 7. Experimental and calculating results of intrusion load and intrusion angle under different friction coefficients of μ_1, ($\mu_2 = 0.25$) 151 × 123 mm (300 × 300 dpi).

Figure 7 shows that when μ_2 is a constant value, the intrusion angle α' increases along with the increasing of μ_1, which means that the intrusion of the ball becomes easier along with the increasing of μ_1.

The real lines in Figures 6 and 7 were drawn according to equation (6). The calculated results indicate that if the values of μ_1 and μ_2 are both constant, when the intrusion angle α' is less than the critical intrusion angle α_{cri}, the ball can intrude without any intrusion normal load. When the intrusion angle α' is larger than the critical intrusion angle α_{cri}, the intrusion of the ball needs an increasing intrusion normal load W' along with the increasing of intrusion angle α'. When μ_1 is constant, the intrusion angle α' will increase with the increasing of μ_2, and the intrusion of the ball becomes easier. Similarly, when μ_2 is constant, the intrusion angle will increase with the increasing of μ_1, the intrusion of the ball also becomes easier.

Though the ball can intrude without any intrusion normal load when the intrusion angle α' is less than the critical intrusion angle α_{cri}, there is no interaction force between the ball and surface 2 at the beginning of the experiment. Therefore, a very small force is needed to trigger off the ball at the beginning. The reason is that when the intrusion angle α' is less than the critical value, the intrusion normal load W' that lead the ball going across is very small and unstable. When the intrusion angle is larger than the critical intrusion angle, the experimental values of intrusion normal force W' are mostly agreed with the calculating ones.

In order to evaluate the intrusion performance of a ball into sliding contact space, the intrusion diagram is showed in Figure 8 according to equation (7). For each couple values of μ_1 and μ_2, there is a specific critical intrusion angle α_{cri}. The critical intrusion angle increases with the increasing of μ_1 and μ_2, and the intrusion of the ball becomes easier. The data points in Figure 8 are the experimental ones, and the lines represent to the calculation results. Apparently, the experimental results are also mostly agreed with the calculating ones. The intrusion diagram shown in Figure 8 is helpful for choosing materials of surfaces 1 and 2 and designing the shape of the space.

DOI: 10.1002/ls

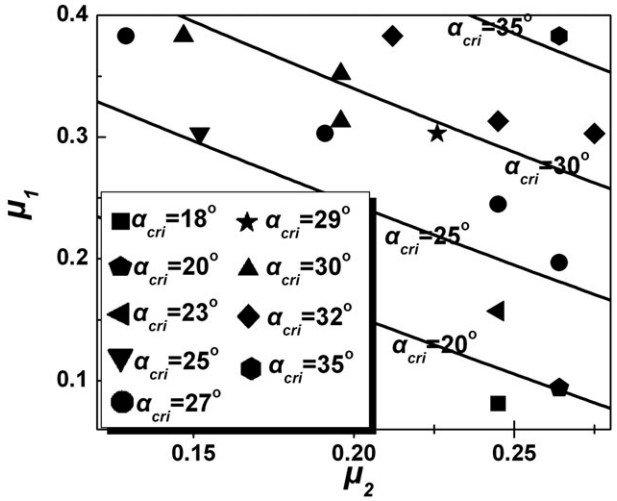

Figure 8. Intrusion diagram of ball into sliding contact space 150 × 117 mm (300 × 300 dpi).

CONCLUSIONS

The intrusion normal load for a ball intruding into sliding contact space depends on the intrusion angle and the friction coefficients between the ball and the two contacting surfaces. There is a critical intrusion angle in the process of intrusion, when the intrusion angle is less than the critical intrusion angle given by equation (8), the ball can intrude without any intrusion normal load; when the intrusion angle is larger than the critical intrusion angle, the intrusion normal load, which is given by equation (6) increases with the increasing of intrusion angle.

NOMENCLATURE

μ_1	friction coefficient between ball and surface 1 (Figure 1)
μ_2	friction coefficient between ball and surface 2 (Figure 1)
W	normal load putting on the centre of ball (Figure 5)
W'	intrusion normal load (when the ball is on the point of getting across the space) (Equation 5)
N_1	normal force between ball and surface 1 (Figure 5)
N_2	normal force between ball and surface 2 (Figure 5)
F_1	friction force between ball and surface 1 (Figure 5)
F_2	friction force between ball and surface 2 (Figure 5)
α	entry angle during the process of ball going forward (Figure 4)
α_0	initial entry angle (Figure 4)
α'	intrusion angle (Figure 4)
α_{cri}	critical intrusion angle (Equation 7)
r	ball radius (Table 1)

DOI: 10.1002/ls

F intrusion force (Equation 3)
E Young's modulus of stainless steel (holder, $E = 2.06*10^{11}$ Pa) (Equation 4)
I Holder's cross section's moment of inertia (Equation 4)
b width of holder's prolongation cross section (14 mm) (Equation 4)
h height of holder's prolongation cross section (0.4 mm) (Equation 4)
d length of holder's prolongation (40 mm) (Figure 4)
d' length of static plate (67 mm) (Figure 4)

ACKNOWLEDGEMENTS

The authors would like to thank the Ricoh Printing System in Japan for support and cooperation and thank the National Nature Science Foundation of China under Grant Numbers of 50775173, the National High-Tech Research and Develop Plan under Grant Number 2007AA04Z307.

REFERENCES

1. Quan H. KOSA study in last 3000 years. *Research of Environmental Science* 1994; **7**(6):1–12.
2. Wu T, Diao D, Xie Y. Study on the dust environment based on tribology. *Lubrication Engineering* 2004; **6**:49–51.
3. Gorana VK, Jain VK, Lal GK. Forces prediction during material deformation in abrasive flow machining. *Wear* 2006; **260**:128–139.
4. Jain RK, Jain VK. Stochastic simulation of active grain density in abrasive flow machining. *Journal Materials Processing Technology* 2004; **152**:17–22.
5. Gorana VK, Jain VK, Lal GK. Experimental investigation into cutting forces and active grain density during abrasive flow machining. *International Journal Machine Tools Manufacture* 2004; **44**:201–211.
6. Jain RK, Jain VK, Dixit PM. Modeling of material removal and surface roughness in abrasive flow machining process. *International Journal Machine Tools Manufacture* 1999; **39**:1903–1923.
7. Jain RK, Jain VK. Simulation of surface generated in abrasive flow machining process. *Robotics Computer Integrated Manufacturing* 1999; **15**:403–412.
8. Liang F, Kun S, Qihong C. Particle movement patterns and their prediction in abrasive flow machining. *Tribotest* 2007; **13**:195–206.
9. Junguo X, Hiromitsu T, Youichi K. Study on soft-particle intrusion in a head/disk interface of load/unload drives. *IEEE Transaction Magnetics*. 2000; **36**(5):2745–2747.
10. Hokkirigawa K, Kato K. An experimental and theoretical investigation of ploughing, cutting and wedging formation during abrasive wear. *Tribology International* 1988; **21**(1):51–57.
11. Briscoe BJ. Isolated contact stress deformations of polymers; the basis for interpreting polymer tribology, in *New Directions in Tribology,* IM Hutchings (ed.), Mechanical Engineering Pub. Ltd.: London, UK, 1997; 191–196.
12. Challen JM, Oxley PLB. An explanation of the different regimes of friction and wear using asperity deformation models. *Wear* 1979; **53**:229–243.
13. Toru M. Tribology in electro-photographic printer. *Tribology in Precision Machines* 2004; **49**:645–650.
14. Wu T, Diao D, Yoshida, K. Wear Characteristics of polymer tapes in ATM tape- scraper tribosystem in sand dust environment. *Proceedings World Tribology Congress III*, Washington, DC, USA, 2005: 909–910.

DOI: 10.1002/ls